Anti-biofouling properties of femtosecond laser-induced sub-micron topographies on elastomeric surfaces

Siddiquiea, Reshma ; Gaddam, Anvesh; Agrawal, Amit; Dimov, Stefan; Joshi, Suhas

DOI:
10.1021/acs.langmuir.0c00753

Document Version
Peer reviewed version

Citation for published version (Harvard):
Siddiquiea, R, Gaddam, A, Agrawal, A, Dimov, S & Joshi, S 2020, 'Anti-biofouling properties of femtosecond laser-induced sub-micron topographies on elastomeric surfaces', *Langmuir*.
https://doi.org/10.1021/acs.langmuir.0c00753

Anti-biofouling properties of femtosecond laser-induced sub-micron topographies on elastomeric surfaces

Reshma Yasmin Siddiquie[a], Anvesh Gaddam[b], Amit Agrawal[a], Stefan S Dimov[b] , Suhas S Joshi[a*].

[a] Department of Mechanical Engineering, Indian Institute of Technology Bombay, Mumbai, India – 400076

[b] Department of Mechanical Engineering, University of Birmingham, Birmingham, UK – B15 2TT

Abstract

Anti-bacterial coatings are often employed to elastomer surfaces to inhibit bacterial attachment. However, such approaches could lead to increased antibiotic resistance. Surface micro/nano texturing is gaining significant attention recently, as it is a passive approach to reduce bacterial adhesion to surfaces. To this end, this work aims to assess the anti-biofouling functionality of femtosecond laser-induced sub-micron topographies on biomedical elastomer surfaces. Femtosecond laser processing was employed to produce two types of topographies on stainless steel substrates. The first one was highly regular and single scale sub-micron laser-induced periodic surface structures (LIPSS) while the second one was multi-scale structures (MS) containing both sub-micron and micron-scale features. Subsequently, these topographies were replicated on Polydimethylsiloxane (PDMS) and Polyurethane (PU) elastomers to evaluate their bacterial retention characteristics. The sub-micron textured PDMS and PU surfaces exhibited long term hydrophobic durability up to 100 hours under the immersed conditions. Both LIPSS and MS topographies on PDMS and PU elastomeric surfaces were shown to substantially reduce (> 89%) the adhesion of gram-negative *Escherichia coli* bacteria. At the same time, the anti-biofouling performance of LIPSS and MS topographies was found to be comparable with that of lubricant-impregnated surfaces. The influence of physical defects on textured surfaces on the adhesion behaviour of bacteria was also elucidated. The results presented here are significant because the polymeric biomedical components that can be produced by replication cost-effectively, while their biocompatibility can be improved through femtosecond surface modification of the respective replication masters.

Keywords: anti-biofouling, biomedical elastomers, femtosecond, laser induced periodic surface structures, lubricant-impregnated surfaces, PDMS, polyurethane.

*Corresponding author: ssjoshi@iitb.ac.in

Introduction

Elastomers are ubiquitous in biomedical devices such as catheters, stents, cardiac pacemaker and contraceptives [1-2]. Microbial infection and thrombosis are major issues that are associated with such biomedical devices, especially those which are synthesised from polyurethanes and silicones [3]. Since the biological responses to elastomeric materials are surface property dependent, many approaches are focused on tailoring the properties of such surfaces. Anti-microbial coatings were though prevalent in inducing bactericidal properties, the increase of antibiotic resistance due to these coatings has become a major concern [4]. Subsequently, the research community was drawn towards renewable polysaccharide-based [5] and nanoparticle-based [6] coatings on elastomeric surfaces. For instance, silver nanoparticle coatings were extensively investigated for imparting anti-bacterial functionality of medical devices [7]. However, recent efforts had shown that the gram-negative bacteria could develop resistance towards these coatings [8]. Furthermore, the coating-based solutions are transient, while their durability and undesirable leaching of metallic ions are some other significant concerns. Another passive and safe-by-design approach that is gaining importance is surface micro-/nano-texturing. In particular, sub-micron and nanotextures reduce the initial attachment on surfaces, thereby inhibiting the formation of biofilms [9].

Surface texturing is a method to create micro/nanoscale topographies on a surface to alter the physical properties like friction [10], reflectivity [11], wettability [12] and hydrodynamic drag [13]. In solid-liquid contacts, the presence of micro or nanoscale topographies results in either completely wetted Wenzel state (WS) or non-wetted Cassie-Baxter state (CBS). These wetting states are characterised by measuring the contact angle (CA) on the surface. The hydrophilic (CA $< 90^{o}$) or hydrophobic (CA $> 90^{o}$) characteristic of a surface is a function of surface chemistry and surface topography. Since the average size of most of the bacteria is in the range of 1-2 μm, surfaces with sub-micron topographies are found to be of anti-biofouling nature [14]. For instance, it was shown that the adhesion of gram-positive bacteria is significantly reduced if the spacing between the protrusions on the surface is less than 1.5 μm [15]. Several investigations have shown that naturally occurring sub-micron topographies on wings of cicada and dragonfly demonstrate anti-bacterial properties [16-17]. Based on the wettability of a surface, the current knowledge about surface topography-induced anti-biofouling characteristics presents two conjectures. The sub-micron textures on a material with high surface energy allow the bacterial suspension to exist in WS. Consequently, sub-micron textures induce stress on bacterial cell wall upon contact, thus

imparting bactericidal characteristics to the surface. On the other hand, the sub-micron or micron-scale topography on a low surface energy material can lead to air entrapment. In such CBS, the bacteria has reduced apparent solid surface area for adsorption and thus its adhesion is inhibited. Another technique for achieving surface functionalisation is to impregnate surfaces with lubricant, referred to as lubricant-impregnated surfaces (LIS). Since the presence of lubricant reduces the apparent solid surface area for bacterial adhesion through adsorption, the LIS were reported to resist a wide range of organisms. In particular, the LIS surfaces were shown to reduce the bacterial adhesion more than 90% and also to offer improved durability over air-cushioned superhydrophobic surfaces [18-19].

To date, among the many approaches to fabricate surfaces with ordered sub-micron textures, exhibiting either hydrophobic or hydrophilic characteristics, etching-based fabrication methods, such as reactive ion etching (RIE) and anodization, have been predominantly employed on different materials. The RIE is used to produce hydrophilic sub-micron protrusions of different lengths, densities and sharpness on black silicon [20-21] and glass [22]. Such surfaces exhibit excellent bactericidal properties through cell membrane rupture. On the other hand, anodization is a relatively cost-effective approach that has been employed to produce porous and protruded sub-micron topographies on various engineering materials such as titanium [23-24] and aluminium [25], and thus to "imprint" anti-biofouling properties on surfaces. Although etching-based fabrication methods are an excellent choice for producing controllable sub-micron textures, these methods are time-consuming, limited to few materials, and utilize chemicals which are not environmental friendly. It is also difficult to produce uniform topographies on complex 3D surfaces using these methods. At the same time, elastomeric and thermoplastic parts of biomedical devices and equipment are commonly produced employing replication methods such as injection moulding, compression and soft moulding [7, 26]. Therefore, it is very important to address any technological gaps in their respective process chains and thus to broaden their use for creating functional sub-micron topographies on surfaces for anti-biofouling applications.

Ultrashort pulse laser surface texturing is an environmentally friendly method that can generate a single scale and hierarchical multiscale topographies on complex 3D surfaces on any substrate material. Several investigations have demonstrated anti-biofouling properties on pico and femtosecond laser textured hierarchical topographies [27-30]. At the same time, low spatial frequency laser-induced periodic surface structures (LIPSS) are gaining much attention recently

as a surface functionalisation method. In particular, such sub-micron topographies have been used successfully to "imprint" a range of attractive properties, such as superhydrophobicity [31], anti-counterfeiting [32], cell proliferation [33] and friction reduction [34], for a number of potential application areas. In addition, a few investigations are reported on the use of LIPSS to create surfaces with anti-biofouling properties. Lutey et al. [35] fabricated two different types of LIPSS (ripples and nanopillars) on stainless steel using femtosecond lasers and demonstrated a reduction in bacterial adhesion by more than 80%. Luo et al. [36] by using a femtosecond laser, generated discontinuous ripples on orthopaedic pure titanium implants and had shown that the bacterial adhesion on textured implants could be reduced by 50%. A more recent investigation of LIPSS on gold surfaces has shown a reduction in bacteria adhesion by almost 99% [37].

In summary, the LIPSS-based sub-micron topographies are potential candidates for "imprinting" anti-biofouling properties on surfaces, along with LIS and etching-based ordered sub-micron topographies. However, their application on elastomers for biomedical applications has not been investigated so far, despite their advantages when they are integrated into high throughput process chains. Therefore, the aim of this research is to investigate systematically the influence of LIPSS on anti-biofouling properties of silicone and urethane-based elastomeric surfaces. In particular, two types of LIPSS topographies were fabricated on steel masters using femtosecond laser processing. The first type was highly regular LIPSS with a periodicity of 800-900 nm [38-39] while the second was a multiscale (MS) topography, i.e. LIPSS superimposed on micron-scale protrusions. Then, these textured steel masters were used to replicate such functional topographies on Polydimethylsiloxane (PDMS) and Polyurethane (PU) elastomers to investigate their bacterial adhesion characteristics against gram-negative *Escherichia coli* bacteria. In addition, the anti-biofouling effectiveness of replicated surfaces was compared with that of lubricant-impregnated surfaces (LIS), as LIS had shown to exhibit excellent inhibition characteristics towards bacteria, too.

Materials and Methods

Fabrication of textured metallic masters

In this study, commercially available AISI 430 (X6Cr17) ferritic stainless steel (SS) plates with 50 x 50 mm^2 surface area, 0.7 mm thick, and average surface roughness of 40 nm were used for producing the textured masters. A LASEA LS5 workstation that integrates a Yb-doped

femtosecond laser source (Satsuma, Amplitude Systemes) with wavelength of 1032 nm, pulse duration of 310 fs, average power of 5W and a maximum pulse repetition rate of 500 kHz has been employed to generate LIPSS, i.e. sub-micron topographies, on the SS plates. The beam delivery system of the workstation is shown in Fig. 1a. Initially, the output beam from the laser source with a diameter of 5 mm is directed through a half-wave plate and a beam expander. Subsequently, the beam is steered through a galvo scan head and a 100-mm focal length telecentric lens at the focal plane with an irradiation spot size ($2R$) of 30 µm.

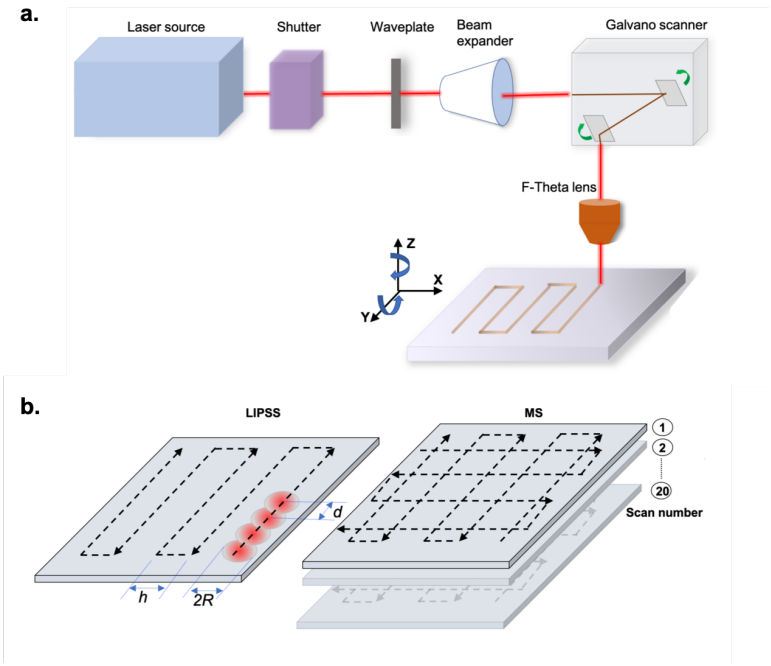

Figure 1: (a) A schematic of the beam delivery system of the laser micro-processing workstation. (b) The scanning strategies to generate LIPSS and MS topographies.

Two types of textured surfaces were fabricated on SS substrates in this research. In the first case, highly regular and single scale LIPSS were fabricated with a bidirectional raster scanning strategy, while in the second case, multiscale (MS) textures consisting of LIPSS superimposed on micron-scale protrusions were fabricated through a grid scanning strategy as shown in Fig. 1b. Initially, small areas up to 3 x 3 mm^2 were textured to optimise the process parameters and thus to generate highly regular LIPSS and shallow MS topographies. The lateral distance between the scan lines (or hatch distance) and average power were varied while scanning speed of 1000 mm/s and repetition rate of 250 kHz were kept constant to obtain highly regular LIPSS. Regarding the MS

topographies, the grid spacing and the number of scan passes were varied when using two different scanning speeds of 1000 and 2000 mm/s while the repetition rate was kept constant at 500 kHz. As a result, grids of surface protrusion with the desired height and spacing of 40 μm were produced. The processing parameters, i.e. repetition rate (*f*), scanning speed (*v*), fluence per pulse (Ø), hatch distance (*h*), scan number and beam polarisation (*e*), used to texture 40 x 40 mm^2 surface areas with LIPSS and MS topographies on SS substrates are given in Table-1. Then, the textured SS substrates were used as masters for soft moulding of PDMS and PU elastomers.

Table-1: Processing parameters used to produce LIPSS and MS topographies.

Topography	Fluence per pulse (mJ/cm^2)	Scanning speed (mm/s)	Hatch (μm)	Repetition rate (kHz)	Layers	Polarisation
LIPSS	250	1000	4	250	1	Linear
MS	430	1000	40	500	20	Linear

Preparation of textured elastomeric surfaces and LIS

The bacterial retention has been analysed on three types of topographies (LIPSS, MS, and LIS) on PDMS and PU replicas. To this end, the LIPSS and MS topographies were replicated on elastomeric surfaces through soft moulding. Initially, Trichloro (1*H*,1*H*,2*H*,2*H*-perfluorooctyl) silane was applied on the textured SS moulds through a vacuum-assisted deposition in a desiccator to facilitate the release of the cured elastomers. In the case of PDMS, a base and a curing agent (Sylgard 184, Dow Corning, USA) were mixed in the ratio of 10:1 and poured onto the silane-treated textured SS moulds. The degassed mixture was allowed to cure for 24 hours. After its hardening, the textured PDMS films were peeled off from the moulds. Regarding the PU replicas, a urethane liquid rubber compound A (4,4′- methylenedicyclohexyl diisocyanate) and B (phenylmercury neodecanoate) with a trade name Clear Flex 50 (Smooth-On, USA), was mixed in the ratio of 1:2. The degassed mixture was then poured again onto silane-treated textured SS moulds and was allowed to cure for 16 hours, before peeling off from the masters. In order to achieve maximum filling of uncured elastomer mixtures in sub-micron cavities of LIPSS and MS topographies, a mild vacuum was applied before the initiation of the curing process. Consequently, the LIPSS and MS topographies were obtained on both PDMS and PU elastomers. In order to prepare LIS, an additional set of MS topographies were moulded on PDMS and PU. These

elastomeric surfaces containing MS topographies were pipetted with silicone oil of 50 cst (Sigma Aldrich) and were allowed to impregnate with the lubricant overnight.

Topography, optical and wettability characterisation

All the textured metallic and elastomeric substrates were first imaged by using a scanning electron microscope (ESEM, Philips FEI Quanta-200, The Netherlands). The dimensional analysis of MS substrates was performed with an optical profilometer (Alicona G5 Infinite focus, Bruker Alicona, Austria). On the other hand, the dimensional measurements of LIPSS substrates were carried out with an Atomic Force Microscope (MFP-3D, Asylum Research, USA), employing a silicon nitride pyramidal probe with a tip radius of 30 nm. The periodicity and regularity of the LIPSS were evaluated by 2D-FFT analysis using Gwyddion open-source image analysis software. The UV-Vis spectra (JASCO, V650, Japan) measurements were conducted from 400 to 700 nm on elastomeric surfaces with LIPSS and MS topographies.

The wetting properties of the textured and LIS substrates were characterised using the sessile droplet method employing contact angle goniometer (Attension Theta, Biolin Scientific, Sweden). The Milli-Q water drops of 5 µl were dispensed under atmospheric conditions on the substrates and the average value of the static contact angle (CA) was obtained. At the same time, the sliding angle (SA) of the droplets on textured and LIS substrates was also measured using the tilting cradle of the goniometer. The longevity of hydrophobic properties of the textured elastomeric substrates was evaluated by measuring the contact angle after submerging them under water for up to 100 hours. The contact angle was measured at fixed intervals on the textured elastomeric substrates after removing them from the water and allowing it to dry in air.

Bacterial retention characterisation

Bacterial adhesion tests were performed on all investigated substrates with a rod-shaped gram-negative bacteria. The *Escherichia coli* BL21 (DE3) strain (Thermofisher Scientific, USA) was selected as an example bacteria in this research because of its wide use in investigations on antimicrobial efficacy of textured surfaces [40-41]. In particular, this motile strain was prepared by first cloning the hplA gene with Green Fluorescent Protein (GFP) in pBSK cloning vector. Then, hplA+GFP was inserted in the pET-28 plasmid vector and was finally transformed into *E.coli* strain to get the robust GFP signal. The *E.coli* bacteria was inoculated in 2 ml of sterilised Luria-Bertani (LB) Broth solution (HiMedia, India). The Chloramphenicol was added to LB broth

to maintain the plasmid vector inside the bacteria strain. Next, the culture was incubated at 37^0C and 155 rpm, for 16 hours to grow the bacteria. The bacterial culture was pelleted down by centrifuging at 3000 rpm for 3 minutes. The obtained pellet was washed three times with 400 µl Phosphate Buffered Saline, pH 7.4, and then resuspended in 600 µl Phosphate Buffered Saline. Finally, the bacterial culture was diluted to a final concentration of 1 x 10^8 cells/ml. Meanwhile, the textured and LIS elastomeric substrates were pre-hydrated in Milli-Q water for 24 hours. The textured substrates were further subjected to mild vacuum to remove the entrapped air. Subsequently, all the substrates were conditioned in Phosphate-buffered saline (PBS) solution for 2 hours before the test to adjust its pH value to 7.4. Bacterial adhesion studies were conducted by placing the plain, textured and LIS substrates (size of 10 mm in diameter) in a 24-well plate containing 0.5 ml of bacterial suspension at 37 °C for 2 hours. Then, the surfaces were washed three times with a PBS solution, to remove any non-adhered bacteria. The adhered bacteria were then fixed by 2.5% of glutaraldehyde for 2 hours. The imaging of the adhered bacteria on the surfaces were performed on a spinning disc confocal microscope (CSU-X1, Yokogawa Electric Corporation, Japan). The obtained fluorescence images were analysed with ImageJ open source software (National Institutes of Health, USA) to quantify the number of bacteria adhering to the surfaces. At least five images per each sample from three replicate experiments were analysed to calculate the mean and standard deviation of the number of adhered bacteria on the surface.

Topographical analysis of textured substrates

The first part of the research reported here is focused on producing highly regular LIPSS and MS topographies on stainless steel using femtosecond laser processing. In order to obtain the highly regular LIPSS, we have chosen a scanning strategy that results in high overlap (O) between two consecutive pulses to avoid any rim effects [42]. The overlap between the pulses was calculated, i.e. $d = v/f$ [31]. By varying the fluence per pulse (Ø) from 100 – 300 mJ/cm^2 and hatch distance from 1 to 5 µm at a fixed overlap of 75%, different LIPSS topographies were achieved in the considered parameter domain. The variation of the hatch distance led to imparting different number of pulses per unit area ($N = \pi R^2/dh$), in particular ranging from 35 to 177. Consequently, the accumulated fluence (Δ = NØ) on the surfaces was in the range of 3.5 – 53.1 J/cm^2. In the considered parameter domain, the LIPSS threshold was observed at an accumulated fluence of 4.4 J/cm^2, while the highly regular LIPSS with a uniform coverage was achieved at 11.1 J/cm^2.

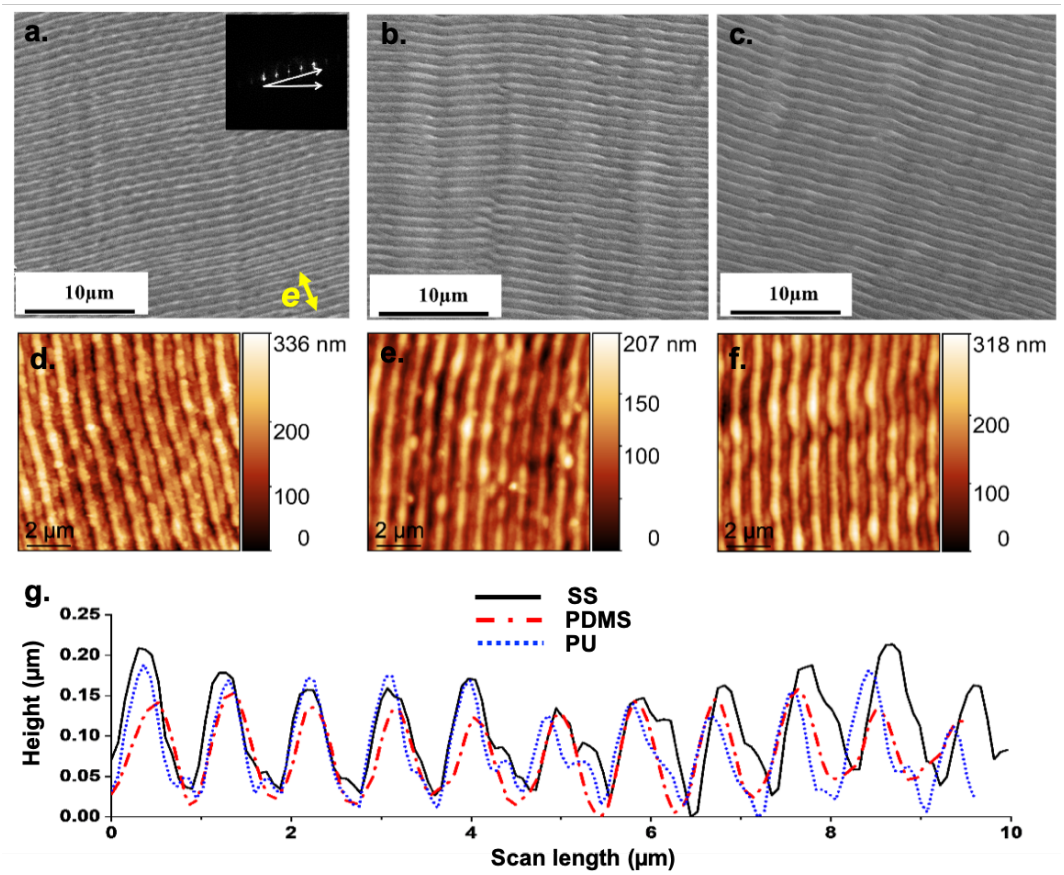

Figure 2: (a-c) The SEM micrographs of highly regular LIPSS on SS, PDMS and PU, respectively. A 2D-FFT image shown in inset of (a). **(d-f)** The AFM micrographs of highly regular LIPSS on stainless steel, PDMS and PU, respectively. **(g)** A plot showing height profiles of highly regular LIPSS on stainless steel, PDMS and PU.

Using the optimal process settings, 40 x 40 mm^2 areas was covered with highly regular LIPSS. On the other hand, MS topographies were produced by creating shallow micron-scale protrusions covered with sub-micron scale LIPSS. The grid scanning strategy resulted in an increased accumulated fluence at the intersecting points, thereby creating a shallow array of micron-scale protrusions. The distance between the intersecting scans and their number was varied from 30 to 50 µm and from 5 to 40, respectively, to produce different MS topographies with varying spacings and heights. However, only the MS topography created with a grid spacing of 40 µm, 20 scans and scanning speed of 1000 mm/s was observed to have smooth profiles without any sporadic holes or defects. The average processing times for covering 40 x 40 mm^2 areas with LIPSS and MS topographies were 6.3 and 12.1 min., respectively.

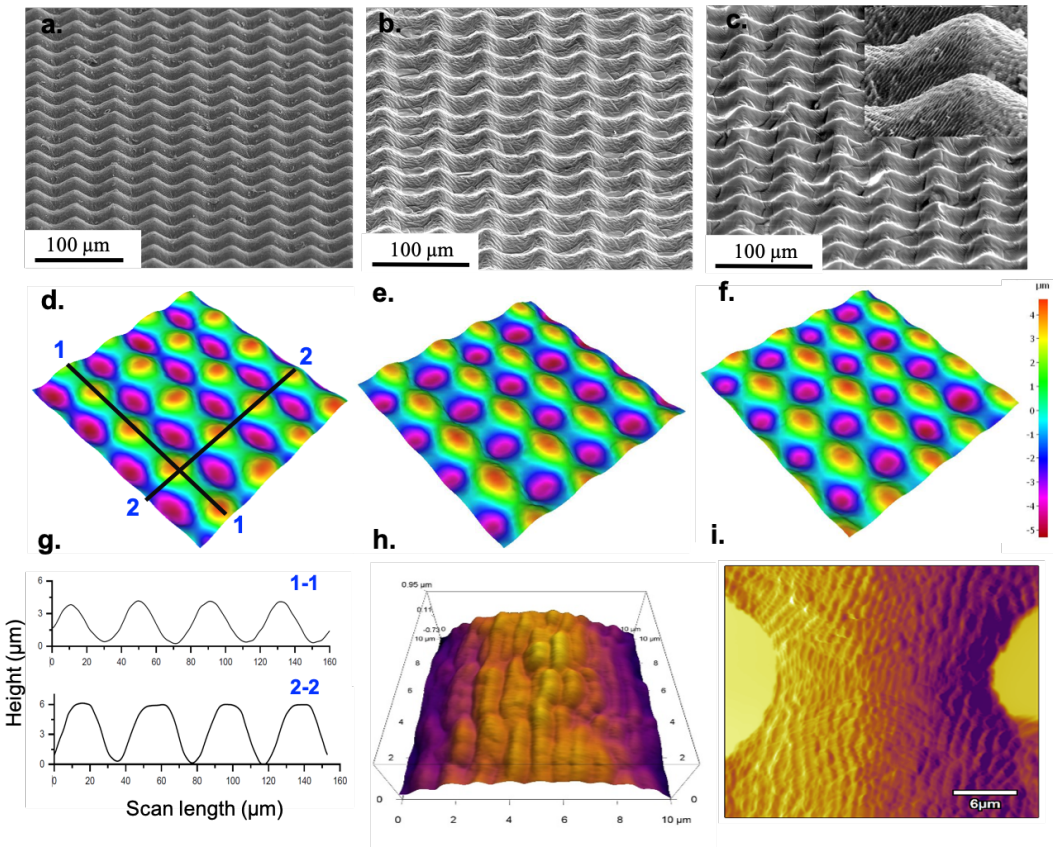

Figure 3: (a-c) The SEM micrographs of MS topographies on SS, PDMS and PU, respectively. **(d-f)** The 3D profiles of MS topographies on of SS, PDMS and PU, respectively. A magnified view of protrusions superimposed with LIPSS shown in inset of (c). **(g)** A plot showing height profiles of micron scale protrusions in different directions. **(h)** The AFM micrograph showing LIPSS on top of the micron scale protrusions. **(i)** The AFM micrograph showing LIPSS in the valley between the consecutive micron scale protrusions.

Fig. 2a shows SEM micrograph of highly regular LIPSS on stainless steel substrates with an orientation normal to the polarisation of the laser irradiation. The periodicity of the LIPSS as evaluated by 2D-FFT (inset of Fig. 2a) is 800-900 nm, which is close to the wavelength of the laser. Furthermore, a clearly defined linear 2D-FFT also signifies the regularity of the LIPSS. It should be noted that the periodicity of the LIPSS is less than the average length (2 µm) of the *E.coli* bacteria [43]. Fig. 2b and c demonstrate the SEM micrographs of negatives replicas of LIPSS topographies on PDMS and PU, indicating an excellent replication. In order to analyse the height of the LIPSS, the AFM measurements were undertaken. Fig. 2d,e, and f show the AFM

micrographs of SS, PDMS and PU LIPSS surfaces with the corresponding depth profiles shown in Fig. 2g. The average height of the LIPSS was in the range from 100 to 200 nm on both SS and elastomer surfaces. By comparing the average heights of three 10 μm scans at different locations on SS and elastomer surfaces, the replication efficiency was estimated to be 87% for PDMS and 93% for PU. The low viscosity of PU (250 cps) when compared with that of PDMS (3500 cps) could be the reason for the discrepancy in replication efficiency.

The SEM micrographs of the MS topographies on metallic and elastomer substrates are illustrated in Fig. 3a, b, and c. It can be seen that the LIPSS are covering consistently the micron-scale protrusions on all substrates without any defects. The 3D images from the optical profilometer on all three substrates are shown in Fig. 3d, e, and f, while the height profiles along the different directions on SS substrate are shown in Fig. 3g. A comparison of height profiles from the measurements has shown a replication efficiency of more than 95% for the MS topographies. The arrangement of LIPSS on top of the protrusions and in the valley on a PDMS substrate is shown in Fig. 3h and i. It can be observed that the height of LIPSS in the MS topographies is from 100 200 nm, too.

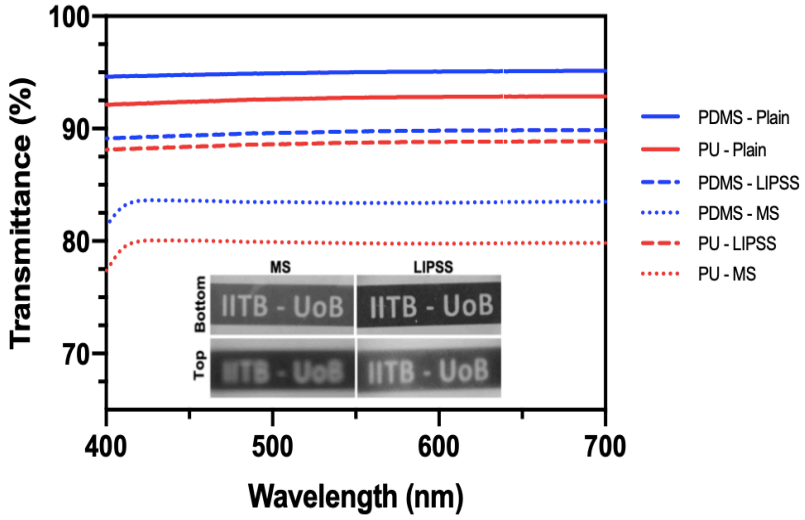

Figure 4: Transmittance spectra of LIPSS and MS topographies on PDMS and PU replicas. Micrographs showing opacity of the LIPSS and MS on PDMS with bottom side facing the logo and on top side away from the logo (inset).

The polymeric surfaces that are susceptible to bacterial fouling in hospitals are either in contact with biological liquids or air [44]. At the same time, elastomers are suitable candidates where

optical transparency is a requirement. Therefore, it is essential to understand the detrimental effects of imparting anti-biofouling functionality on the optical properties of the treated materials. Fig. 4 shows the transmittance plot in the visible wavelength range of plain and textured elastomeric surfaces. The PDMS and PU surfaces have exhibited more than 90% transmittance. While the LIPSS topographies marginally reduced the transmittance, the MS topographies on both elastomers have greater influence (of about 15%) on optical transparency. It is also important to note that the optical transparency depended on the orientation of the textured surface as reported previously [45]. The elastomeric surfaces have shown better opacity if the textured surface faces the object of interest when compared with the case where the textured surface is away from the object of interest (inset of Fig. 4).

Wettability analysis of textured elastomeric surfaces

It is common in biomedical applications, the elastomeric surfaces exposed continuously to liquids, such as bodily fluids and medicinal liquids. Such conditions could affect the topography of the elastomeric surfaces, thereby compromising their anti-biofouling functionality. Therefore, the second part of this research was focused on investigating the physicomechanical integrity of sub-micron topographies under long-term exposures to liquids. For the sake of simplicity, only water was used as a medium in the experiments where it was required to immerse the textured surfaces. The topography changes on both textured elastomers after the immersion in water were correlated with the contact angle.

In the first, Fig. 5a show the static contact angle measurements on plain and textured substrates of stainless steel and elastomers. The contact angle measurements on textured stainless steel substrates were performed after 30 days of ageing in ambient air to allow hydrophilic to hydrophobic transition [46]. As it can be seen, the MS topographies substantially increased the contact angle of the surfaces on all the substrates when compared to the LIPSS topographies. Also, the MS topography on PDMS imparted near superhydrophobicity by increasing the contact angle to $147^{o} \pm 2.3$. A larger area of air entrapment in MS topographies due to the micron scale cavities as compared to the LIPSS could be the reason for an increased hydrophobicity. At the same time, the lubricant-impregnated textured surfaces on all substrates have shown only a marginal increase in the contact angle. The adhesion of water to textured surfaces was also characterised by measuring the sliding angle on the substrates. The plain and LIPSS samples of all substrates

imparted strong pinning of water droplets even at high tilting angles. Illustrations of a droplet pinning at 90° tilt angle on plain and LIPSS PDMS replicas are shown in Fig. 5c and d, respectively. Only on PDMS replicas with MS topographies, a droplet sliding was observed at an angle of 16° ± 2.1(see Fig. 5e), whereas, on SS and PU samples, the droplets were observed to be pinned at 90°. On the other hand, the sliding angle was observed to be less than 5° on LIS SS and elastomeric samples (see Fig. 5f).

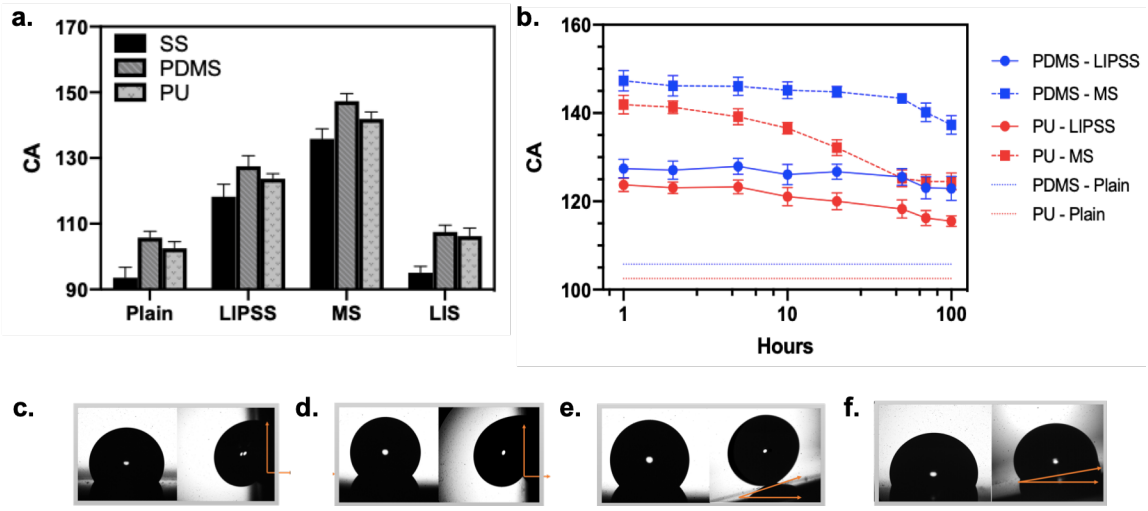

Figure 5: (a) The static water contact angle (CA) on textured and LIS substrates of stainless steel and elastomers. **(b)** A variation of contact angle with immersion time. **(c-f)** The micrographs showing contact angle and sliding angle on plain, LIPSS, MS and LIS topographies of PDMS.

Subsequently, the water immersion experiments were conducted to understand the influence on the hydrophobic properties of the textured elastomeric substrates. This was done by submerging the textured substrates in a container with water level up to a height of 50 mm from the surface, thereby creating a hydraulic pressure of 490 Pa over the substrates. The contact angle was measured on the textured elastomeric substrates at different intervals over 100 hours. Fig. 5b shows the variation in contact angle for LIPSS and MS topographies of PDMS and PU replicas. The contact angles measured on plain substrates were also included in the plot for comparison. It is observed that the contact angle remains reasonably stable for LIPSS topographies on PDMS replicas over the duration of 100 hours. However, the contact angle on MS topographies on PDMS replicas remained stable for 50 hours before beginning to decline. On the other hand, the contact angle for MS and LIPSS topographies on PU decreases gradually, while the rate of decline is

greater in the former. The dissolution of air into the water led to a Cassie-Wenzel transition over a period of time and the rate of this transition depended on the volume of air entrapped in the cavities [47]. As the transition occurs, the water wet the entire surface, thereby degrading either the surface roughness or surface chemistry. Since the textured surfaces have larger contact areas than the plain ones, a change in contact angle would be more pronounced in the former when the degradation occurs [48]. Consequently, the MS topographies although show better hydrophobic properties, are prone to degradation and loss of their hydrophobicity over a continuous exposure to liquids. The contact angles on the plain surfaces of PDMS and PU replicas, however, have not changed significantly in our experiments. Overall, the change in contact angles on textured surfaces was less than 7% and 13% on PU for PDMS replicas, respectively, over a period of 100 hours. Thus, it is evident that the degradation of physicomechanical properties of the textured elastomers is not significant. Consequently, it is expected that the fabricated sub-micron topographies are durable for sufficiently long time in biomedical operating conditions.

Bacterial adhesion on textured and LIS elastomeric surfaces

To determine the anti-biofouling performance of the textured and LIS topographies on the elastomers, *E.coli* bacterial strain was used. Fig. 6a shows the fluorescence micrographs of the adhered *E.coli* bacteria on plain, LIPSS, MS and LIS topographies on PDMS and PU elastomers. It is evident that a large number of bacteria adhere to plain surfaces on both the elastomers. Whereas, the textured and LIS topographies on both PDMS and PU show a significant reduction in bacterial adhesion on them. As shown in Fig. 6b, the reduction in bacterial adhesion on highly regular LIPSS with respect to plain surface is 96.7% and 96.1% for PDMS and PU, respectively. The performance of LIPSS topographies on both elastomers is similar to their respective LIS counterparts. On the other hand, MS topographies on PDMS and PU exhibited a reduction of 91.1% and 89.2% in bacterial adhesion, respectively. In our experiments, the textured substrates were hydrated in water for 24 hours and it was then followed by subjecting them to mild vacuum before conducting bacterial adhesion test. In this way, the Cassie-Wenzel transition was achieved on the surfaces with LIPSS and MS topographies. Subsequently, upon the application of the bacterial suspension on the textured surfaces, the bacteria was brought into contact with the sub-micron topographies as illustrated in Fig. 6a. As a result, the decrease in bacteria-accessible area on LIPSS and MS surfaces when compared to the plain ones, led to a reduction in adhesion. Since the contact area on the MS topography was more effective in regards to the bacteria suspension

than the LIPSS topography, the former exhibited a slightly increased bacterial retention than the latter.

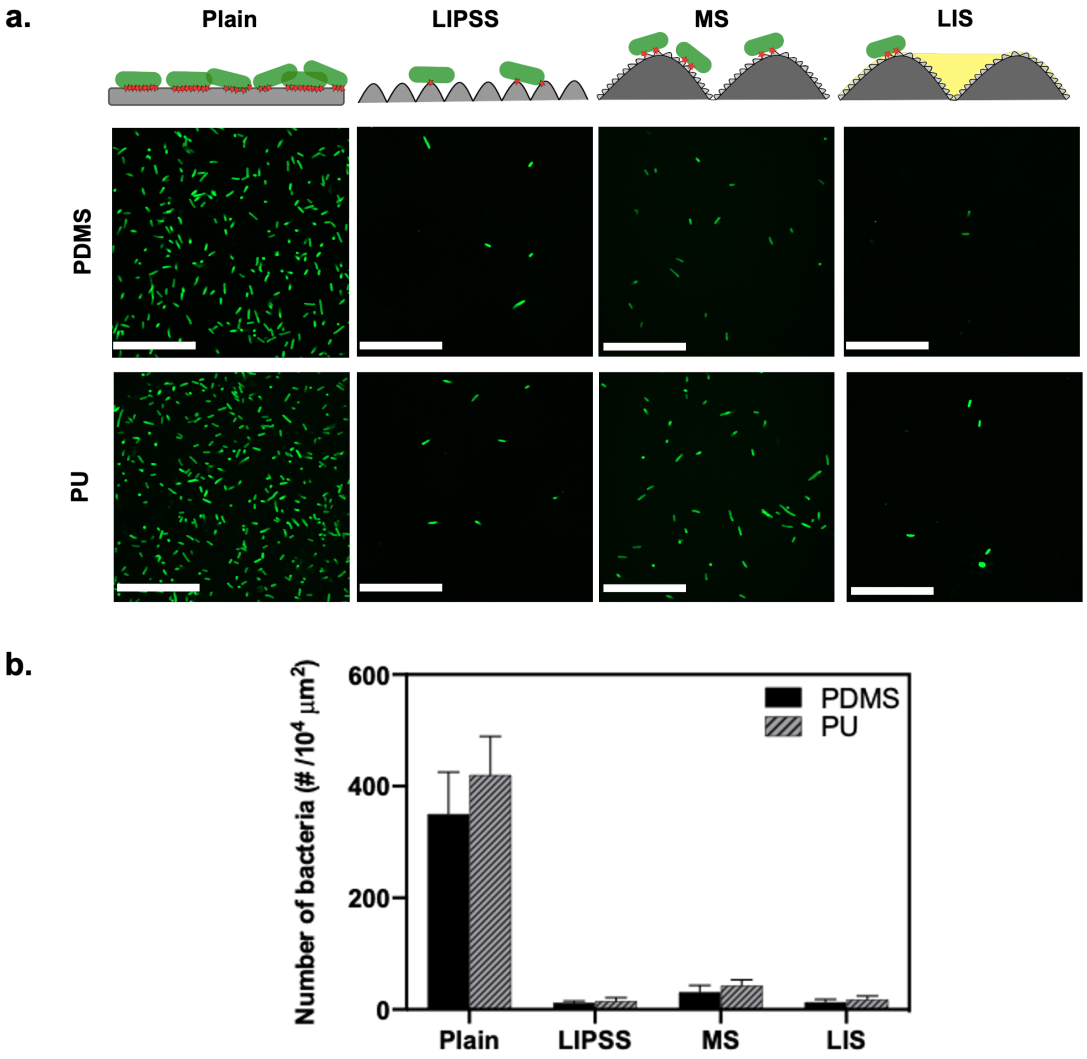

Figure 6: (a) The illustrations of bacteria on difference surfaces is shown (above). The contact points of bacteria on a surface is highlighted in red in these images. The fluorescence micrographs showing bacteria adhesion on plain, LIPSS, MS and LIS topographies of PDMS and PU (below). The scale bar is 25 µm. **(b)** A plot showing the number of bacteria adhered to surfaces on different topographies.

It has been pointed out by some researchers that the disappearance of the air layer on superhydrophobic surfaces led to a decrease of their anti-biofouling performance [49-50]. However, mainly surfaces with micron-scale topographies were investigated, where the surface

features were larger than the size of the bacteria. On micron-scale topographies, the bacterial suspension has increased apparent solid surface area upon reaching the Wenzel state due to the vanished air layer. Therefore, such superhydrophobic surfaces promote bacterial adhesion. On the other hand, the anti-biofouling performance is not a function of the air layer on surfaces with sub-micron topographies [51-52]. Hence, it is important that the mean size of surface features is less than the size of bacteria and thus to minimise the anchorage points for inhibiting bacterial adhesion. For instance, the round-shaped bacteria have shown to be a successful coloniser on surfaces with mean feature sizes marginally greater than their size [35, 53]. As the periodicity of the sub-micron topographies was less than the size of *E.coli* in our experiments, a substantial reduction in bacterial adhesion was achieved. Furthermore, the PDMS has shown slightly better anti-biofouling performance over the PU counterparts. This could be explained with the different stiffness of these two materials. It was shown that the room temperature cured PDMS exhibited a Shore A hardness of 44 [54], while higher values were obtained on PU substrates with hardness of about 50 [55]. Some other results reported that materials with low stiffness exhibit better anti-biofouling properties against E. coli [56-57]. However, it should be stated that there is no consensus among researchers regarding the influence of material stiffness on bacterial adhesion.

Since the SS moulds are susceptible to damage and wear over continuous usage [58-59], it is essential to evaluate the influence of physical defects on surface on the bacterial adhesion. To this end, the SS moulds containing LIPSS and MS topographies were subjected to abrasion tests [60]. Briefly, the sub-micron topographies were subjected to abrasion for 10 cycles on sandpaper (grit no. 600) with a load of 200 g (6.1 kPa) as shown in Fig. 7a. Subsequently, the bacterial adhesion tests were conducted on PDMS surfaces containing worn out LIPSS and MS topographies. An illustration of removal (knock-off) of LIPSS on micron-scale protrusions of MS topographies is shown in Fig. 7a along with the SEM image depicting the worn-out segments on the SS mould with MS topographies in Fig. 7b. The accumulation of bacteria in the valleys between the micron scale protrusions due to defective MS topographies is evident from the fluorescence micrograph in Fig. 7c. Overall, the reduction in bacterial adhesion on ‘worn-out’ LIPSS and MS topographies was found to be only 13.2% and 21.6%, respectively. Since only LIPSS on top of the protrusions worn out during the abrasion test on MS topographies while the underlying LIPSS in the valleys were protected, the MS topographies had shown a slightly low reduction in bacterial adhesion than the highly regular LIPSS topographies.

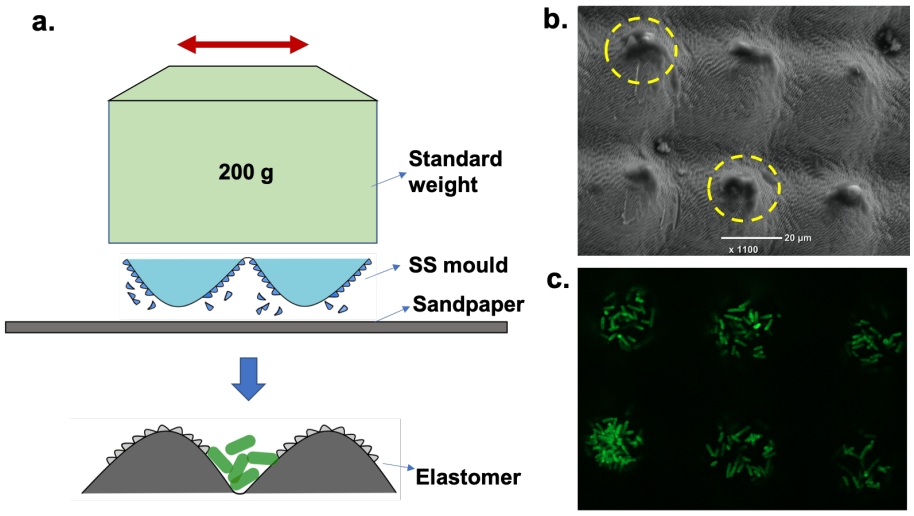

Figure 7: (a) An illustration showing LIPSS "knock-off" from top of the protrusions of a MS topography and bacterial adhesion in valley between the protrusions of replicated substrate. **(b)** A SEM micrograph showing worn out LIPSS from top of the protrusions on MS topography. **(c)** The fluorescence micrograph showing bacteria adhered in the valleys of MS topography.

Concluding remarks

Surface texturing at sub-micron scale is a safe-by-design approach to prevent bacterial fouling, thereby improving biocompatibility of biomaterials. In this work, we have demonstrated that the femtosecond laser-induced sub-micron topographies on PDMS and PU elastomers can induce anti-biofouling properties. Overall, the LIPSS and MS topographies reduced the adhesion of bacteria by more than 89% on both the elastomers. At the same time, the sub-micron textured elastomers exhibited reasonably good durability over long term exposure to the water. Therefore, their anti-biofouling efficacy will be least affected by continuous utilisation in biomedical applications. Although, the LIS have shown to reduce adhesion of bacteria by more than 95%, the functionality of such surfaces is short-lived. This is because lubricant present on the LIS can leach over a period of time into the working liquids and pose contamination issues in biomedical applications. Therefore, highly durable LIPSS or MS topographies can be suitable for such applications. In addition, the LIPSS topographies are optically transparent as compared to MS topographies. However, in reality, fabrication of the LIPSS topographies is sensitive to laser processing disturbances and substrate's surface roughness when compared to the MS topographies. Furthermore, the presence of any small number of physical defects on the LIPSS topographies due

to wear leads to local adhesion of bacteria, thus, compromising their anti-fouling properties. Therefore, the fabrication aspects such as uniform coverage, reproducibility, abrasion resistance and replication efficiency need attention in the case of LIPSS. Altogether, considering the indicators such as a better hydrophobicity, less surface defects and reasonable transparency, despite the high processing time, the MS topographies are better candidates than the highly regular LIPSS for elastomeric surfaces.

Furthermore, it is important to note that the mean feature size of the sub-micron topographies should be less than the typical sizes of the bacteria to achieve the required anti-biofouling response. The near-infrared laser used in this research produced sub-micron topographies with periodicities in the range of 800 – 900 nm, which were less than the size of the rod-shaped *E. coli* bacteria (typical length of 1.5 - 2 μm). At the same time, the typical diameter of the most round-shaped bacteria, e.g. *Staphylococcus spp.* and *S. aureus,* ranges from 0.5 to 1 μm. Therefore, the anti-biofouling performance would be severely compromised on such sub-micron topographies if round-shaped bacteria were used, as they would require a much lower degree of surface contact for a successful adhesion when compared to the rod-shaped bacteria. Therefore, LIPSS with periodicities less than 600 nm would be necessary in order to inhibit adhesion for both bacteria. This could be achieved by varying the laser processing settings, such as laser wavelength, incidence angle and fluence. For example, recently, the LIPSS with periodicities up to 175 nm were produced by using a nanosecond pulsed laser operating at 532 nm wavelength [61]. Since, the geometry, dimensions and periodicity of LIPSS can be tailored in the sub-micron range scale using the laser processing parameters, further studies will be focused on anti-biofouling characteristics of such topographies against both gram-positive and gram-negative bacteria of different shapes and dimensions.

Acknowledgements

Authors are thankful for the financial support of the UKIERI-DST (DST/INT/UK/P-169/2017) and EC H2020 HIMALAIA project. We are also grateful to the instrument support provided by the Sophisticated Analytical Instrument Facility (SAIF) at IIT Bombay, India. We also acknowledge a great help provided by Dr. Himani Sharma, Ms. Vishakha Surve and Prof. Rahul Purwar from the Department of Biosciences and Bioengineering, IIT Bombay, in conducting bacterial retention tests.

References

1. Sheiko, S.S. and Dobrynin, A.V., 2019. Architectural Code for Rubber Elasticity: From Supersoft to Superfirm Materials. *Macromolecules*, 52(20), pp.7531-7546.
2. Claure, I., Anderson, D., Klapperich, C.M., Kuohung, W. and Wong, J.Y., 2019. Biomaterials and Contraception: Promises and Pitfalls. *Annals of Biomedical Engineering*, pp.1-19.
3. Allcock, H.R., 2019. The Background and Scope of Polyphosphazenes as Biomedical Materials. *Regenerative Engineering and Translational Medicine*, pp.1-10.
4. Ahonen, M., Kahru, A., Ivask, A., Kasemets, K., Kõljalg, S., Mantecca, P., Vinković Vrček, I., Keinänen-Toivola, M.M. and Crijns, F., 2017. Proactive approach for safe use of antimicrobial coatings in healthcare settings: opinion of the COST action network AMiCI. *International Journal of Environmental Research and Public Health*, 14(4), p.366.
5. Bračič, M., Mohan, T., Griesser, T., Stana-Kleinschek, K., Strnad, S. and Fras-Zemljič, L., 2017. One-Step Noncovalent Surface Functionalization of PDMS with Chitosan-Based Bioparticles and Their Protein-Repellent Properties. *Advanced Materials Interfaces*, 4(21), p.1700416.
6. Wang, L., Hu, C. and Shao, L., 2017. The antimicrobial activity of nanoparticles: present situation and prospects for the future. *International journal of nanomedicine*, *12*, p.1227.
7. Kim, J.H., Park, H. and Seo, S.W., 2017. In situ synthesis of silver nanoparticles on the surface of PDMS with high antibacterial activity and biosafety toward an implantable medical device. *Nano Convergence*, 4(1), p.33.
8. Panáček, A., Kvítek, L., Smékalová, M., Večeřová, R., Kolář, M., Röderová, M., Dyčka, F., Šebela, M., Prucek, R., Tomanec, O. and Zbořil, R., 2018. Bacterial resistance to silver nanoparticles and how to overcome it. *Nature nanotechnology*, *13*(1), pp.65-71.

9. Xu, L.C., Meyerhoff, M.E. and Siedlecki, C.A., 2019. Blood coagulation response and bacterial adhesion to biomimetic polyurethane biomaterials prepared with surface texturing and nitric oxide release. *Acta Biomaterialia*, 84, pp.77-87.
10. Sharma, H., John, K., Gaddam, A., Navalkar, A., Maji, S.K. and Agrawal, A., 2018. A magnet-actuated biomimetic device for isolating biological entities in microwells. *Scientific Reports*, *8*(1), pp.1-14.
11. Jwad, T., Penchev, P., Nasrollahi, V. and Dimov, S., 2018. Laser induced ripples' gratings with angular periodicity for fabrication of diffraction holograms. *Applied Surface Science*, *453*, pp.449-456.
12. Daniel, D., Lay, C.L., Sng, A., Lee, C.J.J., Neo, D.C.J., Ling, X.Y. and Tomczak, N., 2019. Mapping micrometer-scale wetting properties of superhydrophobic surfaces. *Proceedings of the National Academy of Sciences*, 116(50), pp.25008-25012.
13. Gaddam, A., Agrawal, A., Joshi, S.S. and Thompson, M.C., 2015. Utilization of cavity vortex to delay the wetting transition in one-dimensional structured microchannels. *Langmuir*, *31*(49), pp.13373-13384.
14. Whitehead, K.A., Rogers, D., Colligon, J., Wright, C. and Verran, J., 2006. Use of the atomic force microscope to determine the effect of substratum surface topography on the ease of bacterial removal. *Colloids and Surfaces B: Biointerfaces*, *51*(1), pp.44-53.
15. Wang, Y., Subbiahdoss, G., Swartjes, J., Van Der Mei, H.C., Busscher, H.J. and Libera, M., 2011. Length-Scale Mediated Differential Adhesion of Mammalian Cells and Microbes. *Advanced Functional Materials*, *21*(20), pp.3916-3923.
16. Ivanova, E.P., Hasan, J., Webb, H.K., Truong, V.K., Watson, G.S., Watson, J.A., Baulin, V.A., Pogodin, S., Wang, J.Y., Tobin, M.J. and Löbbe, C., 2012. Natural bactericidal surfaces: mechanical rupture of Pseudomonas aeruginosa cells by cicada wings. *Small*, *8*(16), pp.2489-2494.
17. Kelleher, S.M., Habimana, O., Lawler, J., O'reilly, B., Daniels, S., Casey, E. and Cowley, A., 2016. Cicada wing surface topography: An investigation into the bactericidal properties of nanostructural features. *ACS Applied Materials & Interfaces*, *8*(24), pp.14966-14974.
18. Epstein, A.K., Wong, T.S., Belisle, R.A., Boggs, E.M. and Aizenberg, J., 2012. Liquid-infused structured surfaces with exceptional anti-biofouling performance. *Proceedings of the National Academy of Sciences*, *109*(33), pp.13182-13187.

19. Ware, C.S., Smith-Palmer, T., Peppou-Chapman, S., Scarratt, L.R., Humphries, E.M., Balzer, D. and Neto, C., 2018. Marine antifouling behavior of lubricant-infused nanowrinkled polymeric surfaces. *ACS Applied Materials & Interfaces*, *10*(4), pp.4173-4182.
20. Ivanova, E.P., Hasan, J., Webb, H.K., Gervinskas, G., Juodkazis, S., Truong, V.K., Wu, A.H., Lamb, R.N., Baulin, V.A., Watson, G.S. and Watson, J.A., 2013. Bactericidal activity of black silicon. *Nature Communications*, *4*(1), pp.1-7.
21. Michalska, M., Gambacorta, F., Divan, R., Aranson, I.S., Sokolov, A., Noirot, P. and Laible, P.D., 2018. Tuning antimicrobial properties of biomimetic nanopatterned surfaces. *Nanoscale*, *10*(14), pp.6639-6650.
22. Han, S., Ji, S., Abdullah, A., Kim, D., Lim, H. and Lee, D., 2018. Superhydrophilic nanopillar-structured quartz surfaces for the prevention of biofilm formation in optical devices. *Applied Surface Science*, *429*, pp.244-252.
23. Hizal, F., Zhuk, I., Sukhishvili, S., Busscher, H.J., Van Der Mei, H.C. and Choi, C.H., 2015. Impact of 3D hierarchical nanostructures on the antibacterial efficacy of a bacteria-triggered self-defensive antibiotic coating. *ACS Applied Materials & Interfaces*, *7*(36), pp.20304-20313.
24. Wandiyanto, J.V., Tamanna, T., Linklater, D.P., Truong, V.K., Al Kobaisi, M., Baulin, V.A., Joudkazis, S., Thissen, H., Crawford, R.J. and Ivanova, E.P., 2020. Tunable morphological changes of asymmetric titanium nanosheets with bactericidal properties. *Journal of Colloid and Interface Science*, *560*, pp.572-580.
25. Hizal, F., Rungraeng, N., Lee, J., Jun, S., Busscher, H.J., Van Der Mei, H.C. and Choi, C.H., 2017. Nanoengineered superhydrophobic surfaces of aluminum with extremely low bacterial adhesivity. *ACS Applied Materials & Interfaces*, 9(13), pp.12118-12129.
26. Wu, S., Zuber, F., Maniura-Weber, K., Brugger, J. and Ren, Q., 2018. Nanostructured surface topographies have an effect on bactericidal activity. *Journal of Nanobiotechnology*, *16*(1), p.20.
27. Pan, Q., Cao, Y., Xue, W., Zhu, D. and Liu, W., 2019. Picosecond Laser-Textured Stainless Steel Superhydrophobic Surface with an Antibacterial Adhesion Property. *Langmuir*, *35*(35), pp.11414-11421.
28. Sun, K., Yang, H., Xue, W., He, A., Zhu, D., Liu, W., Adeyemi, K. and Cao, Y., 2018. Anti-biofouling superhydrophobic surface fabricated by picosecond laser texturing of stainless steel. *Applied Surface Science*, *436*, pp.263-267.

29. Epperlein, N., Menzel, F., Schwibbert, K., Koter, R., Bonse, J., Sameith, J., Krüger, J. and Toepel, J., 2017. Influence of femtosecond laser produced nanostructures on biofilm growth on steel. *Applied Surface Science*, *418*, pp.420-424.
30. Li, S., Liu, Y., Zheng, Z., Liu, X., Huang, H., Han, Z. and Ren, L., 2019. Biomimetic robust superhydrophobic stainless-steel surfaces with antimicrobial activity and molecular dynamics simulation. *Chemical Engineering Journal*, *372*, pp.852-861.
31. Romano, J.M., Garcia-Giron, A., Penchev, P. and Dimov, S., 2018. Triangular laser-induced submicron textures for functionalising stainless steel surfaces. *Applied Surface Science*, *440*, pp.162-169.
32. Yao, J., Zhang, C., Liu, H., Dai, Q., Wu, L., Lan, S., Gopal, A.V., Trofimov, V.A. and Lysak, T.M., 2012. Selective appearance of several laser-induced periodic surface structure patterns on a metal surface using structural colors produced by femtosecond laser pulses. *Applied Surface Science*, *258*(19), pp.7625-7632.
33. Martínez-Calderon, M., Manso-Silván, M., Rodríguez, A., Gómez-Aranzadi, M., García-Ruiz, J.P., Olaizola, S.M. and Martín-Palma, R.J., 2016. Surface micro-and nano-texturing of stainless steel by femtosecond laser for the control of cell migration. *Scientific Reports*, *6*, p.36296.
34. Michalek, A., Qi, S., Batal, A., Penchev, P., Dong, H., See, T.L. and Dimov, S., 2020. Sub-micron structuring/texturing of diamond-like carbon-coated replication masters with a femtosecond laser. *Applied Physics A*, *126*(2), p.144.
35. Lutey, A.H., Gemini, L., Romoli, L., Lazzini, G., Fuso, F., Faucon, M. and Kling, R., 2018. Towards laser-textured antibacterial surfaces. *Scientific Reports*, *8*(1), pp.1-10.
36. Luo, X., Yao, S., Zhang, H., Cai, M., Liu, W., Pan, R., Chen, C., Wang, X., Wang, L. and Zhong, M., 2020. Biocompatible nano-ripples structured surfaces induced by femtosecond laser to rebel bacterial colonization and biofilm formation. *Optics & Laser Technology*, *124*, p.105973.
37. Jalil, S.A., Akram, M., Bhat, J.A., Hayes, J.J., Singh, S.C., ElKabbash, M. and Guo, C., 2020. Creating superhydrophobic and antibacterial surfaces on gold by femtosecond laser pulses. *Applied Surface Science*, *506*, p.144952.

38. Garcia-Giron, A., Romano, J.M., Batal, A., Michałek, A., Penchev, P. and Dimov, S.S., 2020. Experimental investigation of processing disturbances in laser surface patterning. *Optics and Lasers in Engineering*, *126*, p.105900.
39. Batal, A., Michalek, A., Garcia-Giron, A., Nasrollahi, V., Penchev, P., Sammons, R. and Dimov, S., 2019. Effects of laser processing conditions on wettability and proliferation of Saos-2 cells on CoCrMo alloy surfaces. *Advanced Optical Technologies*.
40. Wybrańska, K., Paczesny, J., Serejko, K., Sura, K., Włodyga, K., Dziecielewski, I., Jones, S.T., Śliwa, A., Wybrańska, I., Hołyst, R. and Scherman, O.A., 2015. Gold–Oxoborate Nanocomposites and Their Biomedical Applications. *ACS applied materials & interfaces*, *7*(7), pp.3931-3939.
41. Reed, J.H., Gonsalves, A.E., Román, J.K., Oh, J., Cha, H., Dana, C.E., Toc, M., Hong, S., Hoffman, J.B., Andrade, J.E. and Jo, K.D., 2019. Ultrascalable multifunctional nanoengineered copper and aluminum for antiadhesion and bactericidal applications. *ACS Applied Bio Materials*, *2*(7), pp.2726-2737.
42. Tan, B. and Venkatakrishnan, K., 2006. A femtosecond laser-induced periodical surface structure on crystalline silicon. *Journal of Micromechanics and Microengineering*, *16*(5), p.1080.
43. Reshes, G., Vanounou, S., Fishov, I. and Feingold, M., 2008. Cell shape dynamics in Escherichia coli. *Biophysical Journal*, *94*(1), pp.251-264.
44. Adlhart, C., Verran, J., Azevedo, N.F., Olmez, H., Keinänen-Toivola, M.M., Gouveia, I., Melo, L.F. and Crijns, F., 2018. Surface modifications for antimicrobial effects in the healthcare setting: A critical overview. *Journal of Hospital Infection*, *99*(3), pp.239-249.
45. Zahid, A., Dai, B., Hong, R. and Zhang, D., 2017. Optical properties study of silicone polymer PDMS substrate surfaces modified by plasma treatment. *Materials Research Express*, *4*(10), p.105301.
46. Kietzig, A.M., Hatzikiriakos, S.G. and Englezos, P., 2009. Patterned superhydrophobic metallic surfaces. *Langmuir*, *25*(8), pp.4821-4827.
47. Xu, M., Sun, G. and Kim, C.J., 2014. Infinite lifetime of underwater superhydrophobic states. *Physical Review Letters*, *113*(13), p.136103.
48. Varughese, S.M. and Bhandaru, N., 2020. Durability of Submerged Hydrophobic Surfaces. *Soft Matter*. *16*, p.1692-1701.

49. Dou, X.Q., Zhang, D., Feng, C. and Jiang, L., 2015. Bioinspired hierarchical surface structures with tunable wettability for regulating bacteria adhesion. *ACS nano*, *9*(11), pp.10664-10672.
50. Hwang, G.B., Page, K., Patir, A., Nair, S.P., Allan, E. and Parkin, I.P., 2018. The anti-biofouling properties of superhydrophobic surfaces are short-lived. *ACS Nano*, *12*(6), pp.6050-6058.
51. Xu, L.C. and Siedlecki, C.A., 2017. Protein adsorption, platelet adhesion, and bacterial adhesion to polyethylene-glycol-textured polyurethane biomaterial surfaces. *Journal of Biomedical Materials Research Part B: Applied Biomaterials*, *105*(3), pp.668-678.
52. Encinas, N., Yang, C.Y., Geyer, F., Kaltbeitzel, A., Baumli, P., Reinholz, J., Mailänder, V., Butt, H.J. and Vollmer, D., 2020. Submicrometer-Sized Roughness Suppresses Bacteria Adhesion. *ACS Applied Materials & Interfaces*.
53. Fadeeva, E., Truong, V.K., Stiesch, M., Chichkov, B.N., Crawford, R.J., Wang, J. and Ivanova, E.P., 2011. Bacterial retention on superhydrophobic titanium surfaces fabricated by femtosecond laser ablation. *Langmuir*, *27*(6), pp.3012-3019.
54. Johnston, I.D., McCluskey, D.K., Tan, C.K.L. and Tracey, M.C., 2014. Mechanical characterization of bulk Sylgard 184 for microfluidics and microengineering. *Journal of Micromechanics and Microengineering*, *24*(3), p.035017.
55. Zhu, G.J., Ren, P.G., Guo, H., Jin, Y.L., Yan, D.X. and Li, Z.M., 2019. Highly sensitive and stretchable polyurethane fiber strain sensors with embedded silver nanowires. *ACS applied materials & interfaces*, *11*(26), pp.23649-23658.
56. Lichter, J.A., Thompson, M.T., Delgadillo, M., Nishikawa, T., Rubner, M.F. and Van Vliet, K.J., 2008. Substrata mechanical stiffness can regulate adhesion of viable bacteria. *Biomacromolecules*, *9*(6), pp.1571-1578.
57. Kolewe, K.W., Peyton, S.R. and Schiffman, J.D., 2015. Fewer bacteria adhere to softer hydrogels. *ACS applied materials & interfaces*, *7*(35), pp.19562-19569.
58. Romano, J.M., Gulcur, M., Garcia-Giron, A., Martinez-Solanas, E., Whiteside, B.R. and Dimov, S.S., 2019. Mechanical durability of hydrophobic surfaces fabricated by injection moulding of laser-induced textures. *Applied Surface Science*, *476*, pp.850-860.
59. Garcia-Giron, A., Romano, J.M., Batal, A., Dashtbozorg, B., Dong, H., Solanas, E.M., Angos, D.U., Walker, M., Penchev, P. and Dimov, S.S., 2019. Durability and wear resistance of laser-

textured hardened stainless steel surfaces with hydrophobic properties. *Langmuir*, *35*(15), pp.5353-5363.

60. Wang, P., Yang, Y., Wang, H. and Wang, H., 2019. Fabrication of super-robust and nonfluorinated superhydrophobic coating based on diatomaceous earth. *Surface and Coatings Technology*, *362*, pp.90-96.
61. Reinhardt, H.M., Maier, P., Kim, H.C., Rhinow, D. and Hampp, N., 2019. Nanostructured Transparent Conductive Electrodes for Applications in Harsh Environments Fabricated via Nanosecond Laser-Induced Periodic Surface Structures (LIPSS) in Indium–Tin Oxide Films on Glass. *Advanced Materials Interfaces*, *6*(16), p.1900401.3

Table of Contents graphic